Eur. Phys. J. D **46**, 437–442 (2008)
DOI: 10.1140/epjd/e2008-00010-x

THE EUROPEAN PHYSICAL JOURNAL D

High resolution measurement and MQDT analysis of the $5d^9\,6s^2\,np$, nf $(J = 1)$ autoionizing resonances of mercury

M.A. Baig[1,2,a]

[1] Atomic and Molecular Physics Laboratory, Quaid-i-Azam University, 45320 Islamabad, Pakistan
[2] Physikalisches Institut, Universität Bonn, Nussallee 12, 53115 Bonn, Germany

Received 2 October 2007 / Received in final form 13 November 2007
Published online 23 January 2008 –

Abstract. We report new high resolution photoabsorption measurements of the $5d$-subshell excitation spectra of mercury using a 3-meter normal incidence spectrograph equipped with a 6000 line/mm holographic grating and synchrotron radiation emitted by the Bonn 2.5 GeV electron accelerator as the background source of continuum. The observed spectra reveal autoionizing resonances attached to the $5d^9(^2\mathrm{D}_{5/2})6s^2$ and $5d^9(^2\mathrm{D}_{3/2})6s^2$ parent ion levels of mercury. We have analysed the line shapes of the lower members of the $5d^96s^2np$ and nf $J = 1$ autoionizing resonances using the phase shifted formulation of the MQDT and extracted the interaction parameters.

PACS. 32.70.Jz Line shapes, widths, and shifts – 32.80.-t Photon interactions with atoms – 32.80.Dz Autoionization – 32.80.Fb Photoionization of atoms and ions

1 Introduction

The absorption spectrum of mercury above the first ionization threshold is dominated by the autoionizing resonances due to $5d$-subshell excitation. Adjacent to the ionization limit, there exist the leading members of the series attached to the $5d_{3/2}$ ionic level designated as $5d6p$ $^3\mathrm{P}_1$ and $^3\mathrm{D}_1$ respectively whereas the leading member of the $5d_{5/2}$ $6p$ $^1\mathrm{P}_1$ series lies below the first ionization limit and perturbs the principal and inter-combination $6snp$ $^1\mathrm{P}_1$ and $^3\mathrm{P}_1$ series. The spectrum of mercury in the autoionization region has been extensively studied using the photoabsorption technique (Beuttler [1], Marr and Auston [2], Garton and Connerade [3], and Cairns et al. [4], Mansfield [5], Baig [6]). The relative and total photoionization cross sections in the autoionization region was obtained by Brehm [7], Brehm and Hofler [8] and Berkowitz and Lifshitz [9,10]. Dehmer and Berkowitz [11] obtained the partial cross sections for the $6s$ $^2\mathrm{S}_{1/2}$, $5d$ $^2\mathrm{D}_{5/2}$ and $^2\mathrm{D}_{3/2}$ ionic states using the branching ratios together with the normalized total photoionization cross section of Cairns et al. [4], while the partial relative cross section for the individual $6s$ $^2\mathrm{S}_{1/2}$, $5d$ $^2\mathrm{D}_{5/2}$ and $^2\mathrm{D}_{3/2}$ states have been measured by Müller et al. [12].

Martin et al. [13] applied the Slater-Condon theory with configuration interaction to calculate the positions of the energy levels in mercury. Forrest et al. [14] studied the autoionizing states of mercury by electron impact excitation and proposed numerous new assignments to the levels of $5d^96s^2ns$, $5d^96s^26d$, $5d^{10}6p^2$ and $5d^96s^27s$ configurations, based on both theoretical calculations and quantum defect series analysis. The measurement of the spin polarization of photoelectrons in the autoionization region using circularly polarized synchrotron radiation and using un-polarized light from rare gas discharge lamps were reported by Schäfers et al. [15]. The experimental data on the photoabsorption cross section and angle resolved photo-electron spin polarization for mercury have been presented by Schönhense et al. [16]. Müller et al. [12] conducted the spin-polarization measurement in the autoionization region and investigated the angle-resolved photoelectrons between the $5d^96s^2$ $^2\mathrm{D}_{5/2}$ and $^2\mathrm{D}_{3/2}$ thresholds. Bartschat and Scott [17] theoretically calculated the total cross section of mercury in the energy range 10.43 eV to 14.0 eV and also reported the asymmetry parameter (β) for the angular distribution of photoelectrons. Ding et al. [18] employed the two-colour laser spectroscopic technique to excite the inner valence shell spectrum of mercury and observed the multiplet splitting for the $5d^9nf$ states. Schäfers et al. [19] reported a multichannel quantum-defect analysis of the experimental data on the spin-polarization for $6s$ dipole transition amplitudes and phase shift differences for photoionization of $5d$ and $6s$ shells. Recently, Toffoli et al. [20] applied the relativistic time dependent density-functional theory to the photoionization of mercury and calculated the partial cross sections and asymmetry parameter profiles for the $6s$, $5d$, $5p$ and $4f$ sub-shells and compared with the earlier relativistic random phase approximation (RPA) calculations.

[a] e-mail: baig@qau.edu.pk

More recently, the measurements of the angular distribution for the photoionization of mercury into the $5d^9\,{}^2\mathrm{D}_{5/2}$ ionic states has been reported by Zubek et al. [21].

The present work is in continuation of our previous studies on the high resolution d-subshell excitation spectra of group II elements (Sommer et al. [22], Baig et al. [23]). In this contribution we present new high resolution photoabsorption data of neutral mercury in the $5d$-subshell excitation region. As a result of higher dispersion and resolution, the line shapes of the autoionizing resonances lying above the $6s_{1/2}$ ionisation threshold and between the $5d_{5/2}$ and $5d_{3/2}$ ionic limits have been investigated. We have used the phase shifted formalism of the multichannel quantum defect theory (Cooke and Cromer [24]) to parameterise the resonance profiles to extract the inter-channel interaction parameters.

2 Experimental details

The spectra were photographed in the first order of a three meter off plane Eagle mounting spectrograph equipped with a 6000 line/mm holographic grating and the synchrotron radiation emitted by the 2.5 GeV electron accelerator at the Bonn University, Germany served as the background source of continuum. The path length of the absorption column was about 150 cm and the furnace was heated to about 350 to 375 K that correspond to the mercury vapour pressure about 0.3 to 0.8 Torr. The spectra were recorded on the short wavelength range (SWR) plates (Kodak, UK) at a reciprocal dispersion of 0.0523 nm/mm with 15 μm slit. The resolution of the spectrograph is $\approx 0.05\ \mathrm{cm}^{-1}$. The spectra recorded on the photographic plates were digitized with a computer-controlled micro-densitometer. The transmission of the photographic plates was measured in steps of 5 μm using a slit width of 10 μm at the photo-multiplier. The spectra were calibrated in wavelengths using the sharp absorption lines of the hydrogen (Baig and Connerade [25]) and inert gases lying in this region.

3 Results and discussions

The ground state electronic configuration of mercury is $5d^{10}6s^2$ and removal of a $5d$-subshell electron produces two ionic states namely $5d^96s^2\ {}^2\mathrm{D}_{5/2}$ and ${}^2\mathrm{D}_{3/2}$ which lie at 119 698.15 cm^{-1} and 134 736.15 cm^{-1} above the ground state respectively. In the present synchrotron radiation based experiments, the photo-absorption spectra in the $5d$-subshell excitation region from the ground state reveals six $J = 1$ Rydberg series culminating on two limits:

$$\begin{aligned} 6s^2{}^1\mathrm{S}_0 &\rightarrow 5d^9({}^2\mathrm{D}_{5/2})6s^2 \quad & np[3/2]_1 \\ & & nf[1/2]_1, nf[3/2]_1 \\ 6s^2{}^1\mathrm{S}_0 &\rightarrow 5d^9({}^2\mathrm{D}_{3/2})6s^2 \quad & np[1/2]_1, np[3/2]_1 \\ & & nf[3/2]_1. \end{aligned}$$

One np and two nf series are attached to the $5d_{5/2}$ limit whereas two np and one nf series are built on the $5d_{3/2}$ limit. The excited levels are represented using the j_cK-couping scheme (Racah [26], Cowan [27]). In this scheme the orbital angular momentum of the core electrons $j_c = 5/2,\ 3/2$ are weakly coupled with the orbital angular momentum ℓ_2 of the excited electron revealing K-quantum number. K is then weakly coupled with the spin quantum number s_2 of the excited electron giving the resultant J-quantum number. The levels are designated as $n\ell[\mathrm{K}]_J$. The leading member of the $5d_{5/2}6s^2np[3/2]_1$ series with $n = 6$ lies below the first ionization threshold and consequently perturbs the $6snp[1/2]_1$ (${}^3\mathrm{P}_1$ in LS designation) and $6snp[3/2]_1$ (${}^1\mathrm{P}_1$ in LS designation) series. These perturbations occur around $n = 9$ that have been analyzed using the three-channel quantum defect theory in our earlier paper (Baig et al. [28]).

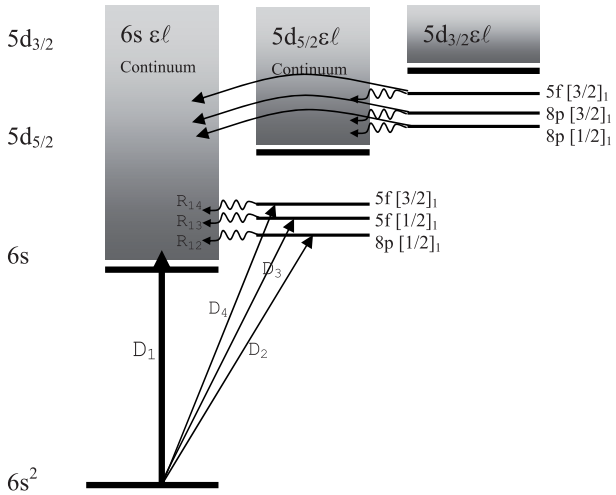

Fig. 1. A schematic diagram showing the pertinent levels and the interaction parameters in terms of MQDT representation. The R_{ij} are the interaction parameters, D_i are the dipole moments connecting the lower state with the upper states and the corresponding open channels in which the quasi discrete levels can decay.

All the other levels attached to the $5d$-innershell excitation lie above the first ionization limit therefore they can decay into the $6s({}^2\mathrm{S}_{1/2})\varepsilon\, J = 1$ continuum. Whereas for the levels that lie in between the $5d_{5/2}$ and $5d_{3/2}$ limits, in addition to the $6s({}^2\mathrm{S}_{1/2})\varepsilon\, p$ continuum the $5d_{5/2}\varepsilon\ell J = 1$ continuum channels also become available for autoionization. In order to determine the inter-channel interactions between the continuum channels and the series attached to the $5d$ limits we present here the treatment of the phase shifted formulation of MQDT (Cooke and Cromer [24]). A schematic diagram of the pertinent levels and the available continua responsible for autoionizing are presented in Figure 1. The interaction parameters R_{ij} and dipole moments connecting the upper and the lower states D_i and the available continua $\varepsilon\,\ell$ for each quasi discrete level are also shown.

First we consider the autoionizing levels attached to the $5d_{5/2}$ limit. The $6s({}^2\mathrm{S}_{1/2})\,\varepsilon\, p$ channel is assigned as a generalized continuum channel, the $5d_{5/2}n\ell$ Rydberg sates mainly decay into this continuum. In Figure 2 we

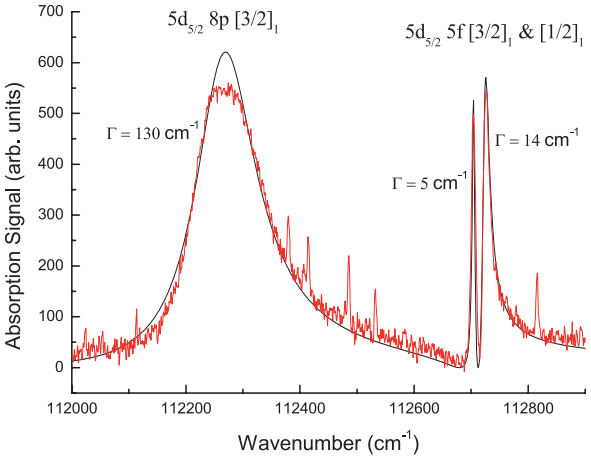

Fig. 2. (Color online) A densitometric trace of the $5d_{5/2}8p$ $[3/2]_1$, $5f[1/2]_1$ and $5f[3/2]_1$ autoionizing resonances of mercury in the energy region 112 000 cm^{-1} (13.886 eV) – 112 900 cm^{-1}(13.998 eV). The solid line is the four channel MQDT simulation.

present a densitometric trace of the absorption spectra in the 112 000–112 900 cm^{-1} region showing the autoionizing resonances attached to the $5d_{5/2}$ threshold. These resonances are assigned as $5d_{5/2}8p[3/2]_1$ and $5d_{5/2}5f[1/2]_1$ and $5d_{5/2}5f[3/2]_1$ respectively in order of increasing energy. The f-resonances are the leading members of these series thus enabling an unambiguous level assignment. The $5d_{5/2}8p[3/2]_1$ is the broadest line whereas the $5d_{5/2}5f[1/2]_1$ line remains relatively sharp. The line shapes are also asymmetric. In the MQDT formalism by Cooke and Cromer [24], the asymmetric line-shapes are a reflection of different dipole moments to the bound and continuum channels and the different phase-shifts of these channels relative to the ground state. The next step is to extract the quantum defects and the interaction parameters which are primarily responsible for the resonance widths. We have used a four-channel QDT formalism as described by Cooke and Cromer [24], Gallagher [29] and Baig and Bhatti [30]. The four channels comprise of a generalized continuum as channel–1, $np[3/2]_1$ channel–2, $nf[1/2]_1$ channel–3 and $nf[3/2]_1$ channel–4. Further it is considered that the interactions among the bound channels are negligible. The four channel quantum defect theory matrix is written as:

$$\begin{pmatrix} \tan\pi(\mu_1+\delta_1) & R_{12} & R_{13} & R_{14} \\ R_{12} & \tan\pi(\mu_2+\delta_2) & 0 & 0 \\ R_{13} & 0 & \tan\pi(\mu_3+\delta_3) & 0 \\ R_{14} & 0 & 0 & \tan\pi(\mu_4+\delta_4) \end{pmatrix} = 0 \quad (1)$$

Here δ_{li} are the eigen quantum defects and R_{ij} are the interchannel interaction parameters. A generalised expression to represent the photoionization cross section with one open and $(n-1)$ bound channels has been derived by Baig and Bhatti [30] as:

$$\sigma = K \frac{\left|\sum_1^n C_{1i}^2 D_i\right|^2}{C_{11}^2 + \left|\sum_2^n C_{1i}^2 R_{1i}\right|^2}. \quad (2)$$

Here C_{1i} are the co-factors of the first row of the MQDT matrix and D_i are the transition dipole moments between the initial state and the ith channel. The summation in the numerator is over all the n-channels involved, while in the denominator the summation is only over the $(n-1)$ bound channels. A comparison between the experimentally observed spectra and the simulated spectra using the following MQDT parameters is shown in Figure 2.

$$\begin{array}{llll} D_1 = -3.0 & D_2 = 6.0 & D_3 = 1.2 & D_4 = 2.0 \\ & \delta_2 = 0.159 & \delta_3 = 0.039 & \delta_4 = 0.033 \\ & R_{12} = 0.23 & R_{13} = 0.05 & R_{14} = 0.08. \end{array}$$

From these extracted MQDT parameters the widths of the autoionizing resonances have been determined using the expression:

$$\Gamma(\text{cm}^{-1}) = \frac{4R_{\text{Hg}}R_{ij}^2}{\pi\nu_2^3}. \quad (3)$$

Here ν_2 is the effective quantum number with respect to the $5d_{5/2}$ ionization limit and R_{Hg} is the mass corrected Rydberg constant for mercury 109 737.315 cm^{-1}. The MQDT parameters show that the interaction between the continuum channel and the $np[3/2]_1$ channel is nearly five times larger than that of the $nf[1/2]_1$ channel and about three times larger than the interaction between the continuum and the $nf[3/2]_1$ channel. The resonance widths of $8p[3/2]_1$ and $5f[1/2]_1$ are determined as 130 (10) cm^{-1} and 5 (1) cm^{-1} respectively whereas, the width of the $5f[3/2]_1$ resonance is 14 (2) cm^{-1}. The reduced widths ($\Gamma_r = \Gamma\nu_2^3$) for these resonances are calculated as 7390 (100) cm^{-1}, 350 (10) cm^{-1} and 875 (10) cm^{-1} respectively.

The corresponding levels attached to the $5d_{3/2}$ limit are, $5d_{3/2}8p[1/2]_1$, $5d_{3/2}8p[3/2]_1$ and $5d_{3/2}5f[3/2]_1$. This part of the spectrum is reproduced in Figure 3 covering the spectral region 126 500–128 000 cm^{-1}. The spectrum can also be represented as a four-channel case as described above. One additional assumption has been made that the generalised continuum contains contribution from the $5d_{5/2}\,\varepsilon\ell$ and $6s_{1/2}\,\varepsilon\ell$ open channels. We define the generalized continuum as channel–1, $8p[1/2]_1$ as channel–2, $8p[3/2]_1$ as channel–3 and $5f[3/2]_1$ as channel–4. The experimentally recorded spectra and the simulated spectra using the four-channel QDT formalism are reproduced in Figure 3 showing excellent agreement. The following MQDT parameters have been used to simulate the spectra.

$$\begin{array}{llll} D_1 = -5.5 & D_2 = 4.6 & D_3 = 1.7 & D_4 = 1.6 \\ & \delta_2 = 0.241 & \delta_3 = 0.171 & \delta_4 = 0.029 \\ & R_{12} = 0.16 & R_{13} = 0.085 & R_{14} = 0.06. \end{array}$$

The widths of the $5d_{3/2}$ $8p[1/2]_1$ and $5d_{3/2}$ $8p[3/2]_1$ resonances are determined as 67 (5) cm^{-1} and 16 (2) cm^{-1} respectively whereas, that of the $5d_{3/2}5$f $[3/2]_1$ resonance as 6 (1) cm^{-1}. The reduced widths of these autoionizing resonances are calculated as 3580 (100) cm^{-1}, 895 (10) cm^{-1}and 390 (10) cm^{-1} respectively. It is

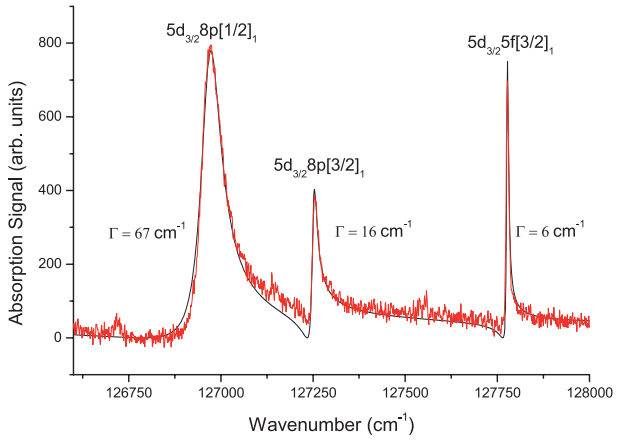

Fig. 3. (Color online) A densitometric trace of the $5d_{3/2}8p$ $[1/2]_1$, $[3/2]_1$ and $5f[3/2]_1$ autoionizing resonances of mercury in the energy region 126 500 cm^{-1} (15.684 eV) – 128 200 cm^{-1} (15.894 eV). The solid line is the four channel MQDT simulation.

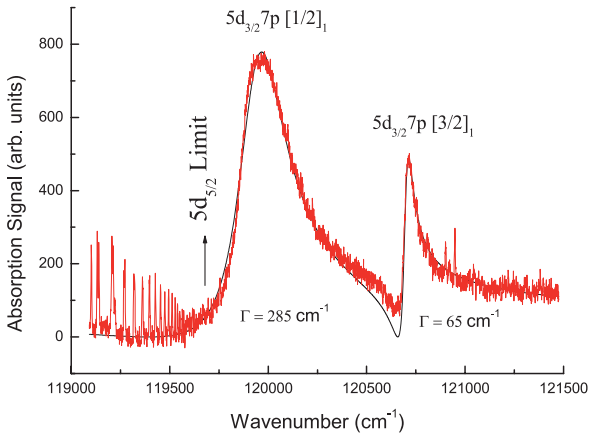

Fig. 4. (Color online) A densitometric trace of the $5d_{3/2}7p[1/2]_1$ and $5d_{3/2}7p[3/2]_1$ autoionizing resonances of mercury in the energy region 119 000 cm^{-1} (14.754 eV) – 121 500 cm^{-1}(15.064 eV). The solid line is the three channel MQDT simulation.

interesting to note that the width of the $5d_{3/2}$ $8p[1/2]_1$ resonance is nearly four times larger than the $5d_{3/2}$ $8p[3/2]_1$ line that means the autoionization rate is much faster in the case of the $5d_{3/2}np[1/2]_1$ channels.

The lowest member of the p-series built on the $5d_{3/2}$ limit observable in the present work ($n = 7$) lies adjacent to the $5d_{5/2}$ limit is shown in Figure 4 covering the energy region from 119 000 cm^{-1}to 121 500 cm^{-1}. In this energy region, in addition to the strongly autoionizing resonances assigned as $5d_{3/2}7p[1/2]_1$ and $5d_{3/2}7p[3/2]_1$, the higher members of the series converging to the $5d_{5/2}$ limit are apparent. It is to remark that here the $5d_{3/2}nf$ resonances are absent as the leading member of this series begins to appear at $n = 5$ which lies adjacent to the $5d_{3/2}8p$ $[1/2]$ and $[3/2]$ lines (see above). To simulate the observed spectra, we have used a three-channel model of the quantum defect theory where the co-factors are described as:

$$\begin{aligned} C_{11} &= (\varepsilon_2\varepsilon_3 - R_{23}^2), \\ C_{12} &= -(\varepsilon_3 R_{12} - R_{13}R_{23}) \quad \text{and} \\ C_{13} &= -(\varepsilon_2 R_{13} - R_{12}R_{23}). \end{aligned} \tag{4}$$

Here ε_i $(i = 1, 2, 3)$ represents $\tan[\pi(\nu_i + \delta_i)]$. Since both the autoionizing resonances are built on the same limit and possess same J-values therefore they are considered as non-interacting. Adjusting the parameter R_{23}= 0 a simple analytical expression for the photoionization cross section is written as:

$$\sigma = \frac{|\varepsilon_2\varepsilon_3 D_1 - \varepsilon_3 R_{12} D_2 - \varepsilon_2 R_{13} D_3|^2}{(\varepsilon_2\varepsilon_3)^2 + |\varepsilon_2 R_{13}^2 + \varepsilon_3 R_{12}^2|^2}. \tag{5}$$

The line profiles of these autoionizing resonances have been simulated using the following MQDT parameters:

$$\begin{array}{lll} D_1 = -7.5 & D_2 = 5.4 & D_3 = 2.0 \\ & \delta_2 = 0.278 & \delta_3 = 0.204 \\ & R_{12} = 0.20 & R_{13} = 0.10. \end{array}$$

A comparison of the experimentally observed spectra and that of the simulated spectra shown in Figure 4 are in excellent agreement. The widths of the $5d_{3/2}7p[1/2]_1$ and $5d_{3/2}7p[3/2]_1$ resonances have been determined as 285 (10) cm^{-1} and 65 (5) cm^{-1} respectively.

Having simulated the observed autoionizing resonances attached to the $5d_{5/2}$ and $5d_{3/2}$ limits, as shown in Figures 2 and 3, we are tempted to compare the interaction strengths of the $5d_{5/2}8p[3/2]_1$ and $5d_{5/2}5f[3/2]_1$ levels and that of the $5d_{3/2}8p[3/2]_1$ and $5d_{3/2}5f[3/2]_1$ levels with their respective continuum channels. The interaction parameters (R_{ij}) for the $5d_{5/2}8p[3/2]_1$ level is 0.23 and that of the $5d_{3/2}8p[3/2]_1$ level is 0.085, nearly 63% small. Whereas, the interaction parameters for the $5d_{5/2}5f$ $[3/2]_1$ and the $5d_{3/2}5f[3/2]_1$ levels are 0.08 and 0.06 respectively, about 25% small. The observed width of the $5d_{5/2}8p[3/2]_1$ line is nearly eight times larger than the corresponding $5d_{3/2}8p[3/2]_1$ line which shows that the autoionization of the $5d_{5/2}8p[3/2]_1$ level into the continuum is much faster than the $5d_{3/2}8p[3/2]_1$ level. It is to be remarked that the available continuum for the $5d_{5/2}8p[3/2]_1$ level decay is $6s\varepsilon p$ whereas for the $5d_{3/2}8p[3/2]_1$ level the available continua are $6s\varepsilon p$ and $5d_{5/2}\,\varepsilon p$. In is evident that that the additional continuum available to the $5d_{3/2}8p[3/2]_1$ line doesn't enhance its autoionization rate.

The MQDT parameters extracted from the interactions in the discrete region can also be correlated to that extracted from the line shape analysis of the autoionizing resonances. In our previous paper (Baig et al. [28]) we studied the perturbations among the $6snp[1/2]_1$, $np[3/2]_1$ and $5d_{5/2}6p[3/2]_1$ series and determined the interaction parameters $R_{12} = 0.182$ and $R_{13} = 0.05$. However, from the analysis of the interactions between the continuum channel and the $5d_{5/2}8p[3/2]_1$ autoionizing level the interaction parameter is determined as 0.23. Since above the threshold the $6s\varepsilon p$ $[1/2]$ and $[3/2]$ $J = 1$ channels are open therefore the predicted width parameter from the series perturbation analysis will be $\sqrt{R_{12}^2 + R_{13}^2}$, which

Table 1. MQDT parameters for the $5d_{5/2\,,3/2}$ $8p$ and $5f$ autoionizing resonances in mercury.

Assignments	R_{1j}	δ_i	ν	Energy (cm^{-1})	Γ_r (cm^{-1})	$\nu^3\,\Gamma$ (cm^{-1})
$5d_{5/2}8p[3/2]_1$	0.23	0.159	3.841	11 2269	130(10)	7390(100)
$5d_{5/2}$ $5f[1/2]_1$	0.05	0.039	3.961	112704	5(1)	350(10)
$5d_{5/2}$ $5f[3/2]_1$	0.08	0.033	3.967	11 2727	14(2)	875(10)
$5d_{3/2}$ $8p[1/2]_1$	0.161	0.241	3.758	12 6974	67(5)	3580(100)
$5d_{3/2}$ $8p[3/2]_1$	0.085	0.171	3.829	12 7256	16(2)	895(10)
$5d_{3/2}$ $5f[3/2]_1$	0.06	0.029	3.971	12 7782	6(1)	390(10)

Table 2. MQDT parameters for the $d_{3/2}np[3/2]_1$ and $[1/2]_1$ ($n = 7, 8, 9$) autoionizing resonances.

Parameter	$7p[3/2]_1$	$8p[3/2]_1$	$9p[3/2]_1$	$7p[1/2]_1$	$8p[1/2]_1$	$9p[1/2]_1$
R_{1j}	0.10	0.085	0.085	0.20	0.161	0.151
δ_i	0.204	0.171	0.156	0.278	0.241	0.224

Table 3. Comparison of the Fano-parameters with the theoretical calculations.

Resonances $5d_{3/2}np, nf$		E_r(cm^{-1})		Γ (cm^{-1})		q	
		Present work	RTDDFT	Present work	RTDDFT	Present work	RTDDFT
$7p$	$[1/2]_1$	119940	122088.1	280 (10)	84.3	5	6.305
	$[3/2]_1$	120715	122943.0	65 (5)	20.2	5	5.567
$8p$	$[1/2]_1$	126970	127782.3	67 (5)	25.7	5	5.548
	$[3/2]_1$	127253	128113.0	16 (2)	5.9	2.5	5.606
$5f$	$[3/2]_1$	127776.5	129048.6	6 (1)	0.03	5	144.216

RTDDFT: Relativistic time-dependent density-functional-theory, Toffoli et al. (2002) [20].

turns out to be 0.192 and the reduced width for the $5d_{5/2}np[3/2]_1$ resonances is predicted as 5150 (20) cm^{-1}. The reduced widths from the line shape analysis of the $5d_{5/2}8p[3/2]_1$ autoionizing resonance is found to be 7390 (100) cm^{-1}, which is nearly 40% higher than the predicted width from the analysis in the discrete region. This difference may be attributed to the energy dependence of the MQDT parameters which have been noticed from the line shape analysis of the higher members of these series. We collect the relevant data of these resonances in Table 1. The first column represents the level assignments and the other columns represent interaction parameters, quantum defects, effective quantum numbers, resonance energies, resonance widths and the reduced widths respectively.

Next we consider the change in the interaction parameters as a function of the principal quantum number. These parameters for the $np[3/2]_1$ and $np[1/2]_1$ resonances ($7 \leqslant n \leqslant 9$) attached to the $5d_{3/2}$ ionic level are listed in Table 2. The interaction parameters R_{ij} for $np[3/2]_1$ and $np[1/2]_1$ decrease with increasing the principal quantum number. The interaction parameters and quantum defect values approach asymptotic values at higher n-values.

In a recent paper Toffoli et al. [20] reported the theoretical values of the Fano parameters of the leading members of the $5d^9np$ autoionizing states in mercury and the parameters were compared with the experimental values, where available. Since in the present high resolution study we have also extracted the Fano parameters from the line fitting procedure, we present a comparison between the experimental and the theoretical values in Table 3. Interestingly, the theoretical calculations predict the resonance energies about 2000 cm^{-1} and 800 cm^{-1} higher than the experimental energies for $n = 7$ and 8 respectively and the widths are predicted nearly 70% smaller than the experimentally observed values. However, the q-parameters are reasonably in agreement except for the $5f$-state which is predicted to be Lorentzian whereas our experimental data show clearly asymmetric line shape (see Fig. 2). More recently, Zubek et al. [21] have measured the angular distribution for the photoionization of mercury in to the $5d_{5/2}$ ionic state over the energy range from 15 eV to 17 eV at a resolution of 3 meV resolution. The line shape of the dominating $np[1/2]_1$ autoionizing resonance is asymmetric with a clear minima in the cross section. The corresponding data observed in the present work is in good agreement to that of Zubek et al. [21] and Bartschat and Scott [17]. All the three auoionizing resonances show evidently asymmetric line shapes that reflect the superiority of the high resolution studies to unveil the true line shapes.

Having determined the MQDT parameters from the lower members of the series, it is tempting to simulate the entire Rydberg series of the autoionizing resonances between the $5d_{5/2}$ and $5d_{3/2}$ limits. The higher members ($10 \leqslant n \leqslant$ limit) of the series are reproduced in Figure 5, showing the $5d_{3/2}\,np[1/2]_1$, $np[3/2]_1$ and $nf[3/2]_1$ Rydberg series covering the energy region between 131 000–135 000 cm^{-1}. The spectrum has been simulated using the MQDT parameters as derived from the lower members of these series. The simulated spectrum is intentionally displaced from the observed spectrum for a

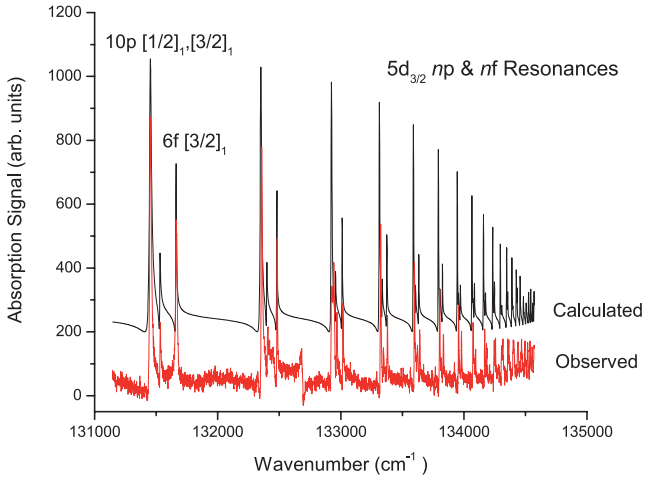

Fig. 5. (Color online) Experimentally observed and the simulated $5d_{3/2}\,np[1/2]_1$, $[3/2]_1$ and $nf[3/2]_1$ autoionizing resonances in mercury covering the energy region 131 000 cm^{-1} (16.242 eV) – 135 000 cm^{-1} (16.738 eV). The parameters used in the simulation are the same as determined from the lower members of the series listed in the text.

meaningful comparison. The excellent agreement between the two spectra demonstrates the supremacy of the phase shifted formalism of the multi-channel quantum defect theory Cooke and Cromer [24] that with only a couple of parameters, one can generate the entire Rydberg series.

In conclusion, we have presented new high resolution data on the autoionizing resonances attached to the $5d$-innershell excitation in mercury. We have presented the MQDT analysis by simulating the observed line profiles and also correlated the MQDT parameters determined below and above the first ionization threshold of mercury. It will be interesting to extend these studies using multi-step laser excitations for the even and odd parity autoionizing states and to determine the absolute value of the photoionization cross section at and above the first ionization threshold.

I am grateful to Prof. J. Hormes at the Physikalisches Institut der Universitat Bonn and Prof. J.P. Connerade at Imperial College, London for their constant support and encouragement. I am also thankful to the Alexander von Humboldt Foundation for the financial support to conduct the experimental work at the Bonn University, Germany.

References

1. J. Beutler, Z. Phys. **86**, 710 (1933)
2. G.V. Marr, J.M. Auston, J. Phys. B **2**, 107 (1969)
3. W.R.S. Garton, J.P. Connerade, Astrophys. J. **155**, 667 (1969)
4. R.B. Cairns, H. Harrison, R.I. Schoen, J. Chem. Phys. **53**, 96 (1970); J.P. Connerade, *Highly Excited Atoms* (Cambridge University Press, 1998)
5. M.W.D. Mansfield, Astrophys. J. **180**, 1011 (1973)
6. M.A. Baig, J. Phys. B **16**, 1511 (1983)
7. B. Brehm, Z. Phys. **21**, 196 (1966)
8. B. Brehm, K. Hofler, Phys. Lett. A **68**, 437 (1978)
9. J. Berkowitz, C. Lifshitz, J. Phys. B **1**, 438 (1968)
10. J. Berkowitz, *Photoabsorption, Photoionization and Photoelectron Spectroscopy* (Academic Press, 1979)
11. J.L. Dehmer, J. Berkowitz, Phys. Rev. A **10**, 48 (1974)
12. M. Müller, F. Schäfers, N. Bowering, C. Hakenkamp, U. Heinzmann, Phys. Scr. **35**, 459 (1987)
13. W.C. Martin, J. Sugar, J.L. Tech, Phys. Rev. A **6**, 2022 (1972)
14. L.F. Forrest, R. Sokhi, V. Pejcev, K.J. Ross, M. Wilson, J. Phys. B **18**, 4519 (1985)
15. F. Schäfers, G. Schonhense, U. Heinzmann, Z. Phys. A **304**, 41 (1982)
16. F. Schönhense, C. Schäfers, U. Hakenkamp, M.A. Heinzmann, Baig, J. Phys. B **17**, L771 (1984)
17. K. Bartschat, P. Scott, J. Phys. B **18**, 3725 (1985)
18. R. Ding, W.G. Kaenders, J.P. Marangos, N. Shen, J.P. Connerade, M.H. Hutchinso, J. Phys. B **22**, L251 R (1989)
19. F. Schäfers, C. Hakenkamp, M. Müller, V. Radojevic, U. Heinzmann, Phys. Rev. A **42**, 2603 (1990)
20. D. Toffoli, M. Stener, P. Decleva, Phys. Rev. A **66**, 012501 (2002)
21. M. Zubek, D.B. Thompson, P. Bolognesi, Cooper, G.C. King, J. Phys. B **38**, 1657 (2005)
22. K. Sommer, M.A. Baig, J. Hormes, Z. Phys. D **4**, 313 (1987)
23. M.A. Baig, M. Akram, S.A. Bhatti, K. Sommer, J. Hormes, J. Phys. B **27**, 1693 (1994)
24. W.E. Cooke, C.L. Cromer, Phys. Rev. A **32**, 2725 (1985)
25. Baig M.A, J.P. Connerade, J. Phys. B **18**, L809 (1985)
26. G. Racah, Phys. Rev. **61**, 537 (1942)
27. R.D. Cowan, *Theory of Atomic Structure, Spectra* (Univ. California Press, 1981)
28. M.A. Baig, R. Ali, S.A. Bhatti, J. Opt. Soc. Am. **14**, 731 (1997)
29. T.F. Gallagher, *Rydberg Atoms* (Cambridge University Press, 1994)
30. M.A. Baig, S.A. Bhatti, Phys. Rev. A **50**, 2750 (1994)